



# Analysis of semi-staggered finite-difference method with application to Bingham flows <sup>☆</sup>

Maxim A. Olshanskii <sup>\*</sup>

Department of Mechanics and Mathematics, Moscow State M.V. Lomonosov University, Vorob'evy Gory 1, Moscow 119899, Russia

## ARTICLE INFO

### Article history:

Received 20 June 2008

Received in revised form 26 October 2008

Accepted 5 November 2008

Available online 27 November 2008

### MSC:

65N06

65N12

74C10

76D07

### Keywords:

Semi-staggered grid

Stabilized discretization

Bingham fluid

Visco-plastic flow

Stokes problem

Iterative methods

## ABSTRACT

In this paper, a finite-difference scheme for incompressible flow problems is treated. The scheme uses non-staggered grid for velocity approximation. A special stabilization is introduced to ensure the well-posedness and optimal approximation properties of the scheme. The stability estimate is proved in the form of a mesh-independent bound for the norm of discrete operator inverse. The finite-difference method is particularly suitable for problems in which velocity vector is involved in additional quantities that enter the system of flow equations as, for example, in the Bingham problem. We describe this application in the paper in some detail. Results of numerical experiments are included that confirm the applicability and optimality of the method.

© 2008 Elsevier B.V. All rights reserved.

## 1. Introduction

Non-staggered grid finite-difference and finite-volume methods are attractive alternatives to staggered grid discretizations of incompressible flow problems when numerical simulations involve complex domains, curvilinear coordinates and immersed interfaces [27,33,37]. For this reason non-staggered approximations have been considered by different authors, see, e.g. [2,36] and the references therein. The non-staggered (or semi-staggered) methods become even more appealing for problems in which velocity vector or its gradient tensor are involved in additional quantities that enter the system of flow equations. This is the case for non-Newtonian flow problems where such grid approximations were found to be particularly convenient from the point of view of data structure and algorithmic simplicity [32,23]. At the same time, non-staggered grid approximations have a well-known stability issue for incompressible flow problems, which has to be addressed (see Section 2). A finite-difference scheme for the Stokes problem

which uses one grid for all velocity components and another grid in elements centers for pressure can be found in the earlier paper [17] (such schemes are also referred in the literature as half-staggered or semi-staggered). However, a rigorous convergence analysis of non-staggered grid approximations is still somewhat lacking. The present paper introduces a stabilization procedure and provides rigorous analysis of the resulting scheme for the particular case of the Stokes problem. We also apply the method for the Bingham flow problem. This model is briefly described below.

A variety of materials exhibits a visco-plastic medium behavior: they combine the behavior of solids in the so-called “rigid” regions, where a certain value of yield stress is not exceeded, and of non-Newtonian fluids in the “flow” regions. For numerical modeling of visco-plastic materials the Bingham model is extensively used in last years, see, e.g. the review article [13]. Naturally emerged from the computational elasticity most of the existing numerical approaches for the Bingham problem use the finite element discretization method. However the integration of this model as a part of existing CFD tools often calls for finite volume or finite difference approximations. This paper is concerned with finite difference solutions for slow steady Bingham flows.

Let  $\Omega \in \mathbb{R}^d$ ,  $d = 2, 3$  be a bounded connected domain. Consider the following system of equations

<sup>☆</sup> This work was supported by the German Research Foundation and the Russian Foundation for Basic Research through Projects 08-01-00159 and 08-01-91957.

<sup>\*</sup> Tel.: +7 495 3355855.

E-mail address: [Maxim.Olshanskii@mtu-net.ru](mailto:Maxim.Olshanskii@mtu-net.ru)

$$\begin{aligned}
 -\operatorname{div} \boldsymbol{\tau} + \nabla p &= \mathbf{f} \text{ on } \Omega, & (1) \\
 \operatorname{div} \mathbf{u} &= 0 \text{ on } \Omega, & (2) \\
 \mathbf{u} &= \mathbf{u}_b \text{ on } \partial\Omega, & (3)
 \end{aligned}$$

and constitutive relation

$$\begin{aligned}
 \boldsymbol{\tau} &= 2\mu \mathbf{D}\mathbf{u} + \tau_s \frac{\mathbf{D}\mathbf{u}}{|\mathbf{D}\mathbf{u}|}, \text{ if } |\mathbf{D}\mathbf{u}| \neq 0, & (4) \\
 |\boldsymbol{\tau}| &\leq \tau_s, \text{ if } |\mathbf{D}\mathbf{u}| = 0,
 \end{aligned}$$

where  $\mathbf{u}, p, \boldsymbol{\tau}$  are unknown velocity, pressure and stress tensor,  $\mu$  is a constant plastic viscosity,  $\tau_s$  is the yield stress,  $\mathbf{u}_b$  is a velocity prescribed on the boundary of  $\Omega$ , such that  $\int_{\partial\Omega} \mathbf{u}_b \cdot \mathbf{n} = 0$ ;  $\mathbf{D}\mathbf{u} = \frac{1}{2}[\nabla \mathbf{u} + (\nabla \mathbf{u})^T]$  is the rate of deformation tensor and

$$|\mathbf{D}\mathbf{u}| = \left( \sum_{1 \leq i, j \leq d} |D_{ij} \mathbf{u}|^2 \right)^{\frac{1}{2}}.$$

We note that constitutive relation (4) can be written in the equivalent form:

$$\mathbf{D}\mathbf{u} = \begin{cases} \left(1 - \frac{\tau_s}{|\boldsymbol{\tau}|}\right) \frac{\boldsymbol{\tau}}{2\mu}, & \text{if } |\boldsymbol{\tau}| > \tau_s, \\ 0, & \text{if } |\boldsymbol{\tau}| \leq \tau_s. \end{cases}$$

For  $\tau_s = 0$  the system (1)–(4) reduces to the Stokes problem. If  $\tau_s > 0$  the relations (1)–(3) hold only in the flow regions, where  $\mathbf{D}\mathbf{u} > 0$ , and make no sense in the rigid region  $\Omega_r = \{\mathbf{x} \in \Omega | \mathbf{D}\mathbf{u}(\mathbf{x}) = 0\}$ .

Applying a finite-difference method to (1)–(4) encounters several difficulties. Thus a grid domain, where the discrete analog of (1)–(3) should be imposed, is not known *a priori* and finding it is a part of the problem. One way to avoid this difficulty is to regularize (4) introducing a function  $\eta_\epsilon(\mathbf{x}) : \mathbb{R}^{d \times d} \rightarrow \mathbb{R}^{d \times d}$  such that  $\eta_\epsilon(\mathbf{x}) \rightarrow 2\mu \mathbf{x} + \tau_s \frac{\mathbf{x}}{|\mathbf{x}|}$  for  $\epsilon \rightarrow 0$  and setting  $\boldsymbol{\tau} = \eta_\epsilon(\mathbf{D}\mathbf{u})$  for some small  $\epsilon$  instead of (4), see [5,28]. This enables one to consider a discrete system of equation approximating a non-Newtonian fluid model in the whole computational domain, thus conventional (iterative) solvers can be applied, e.g. [15,25]. The regularization, however, can introduce additional modeling errors [13], and has the issue of (non)linear solvers efficiency for  $\epsilon \rightarrow 0$ . In this paper, we consider a finite-difference approximation of the non-regularized model (1)–(4). We build an iterative method on the variational inequality and augmented Lagrangian approach of Lions, Glowinski et al. [14,18] previously used for finite element approximations, see Section 4. In finite difference setting this approach requires additional consistency terms to be introduced in the algorithm.

The remainder of the paper is organized as follows: Section 2 presents the finite-difference scheme. The scheme was first considered in [17] for the Stokes problem and in [23] for the Bingham problem. It uses one grid for all velocity components and one grid for pressure and all stress and the rate of deformation tensors components. We discuss the stability issue and propose the stabilization techniques. In Section 3, we show that the scheme is stable for the particular case of the Stokes problem. The stability estimate is proved in the form of a mesh-independent bound for a norm of the discrete operator inverse. From the stability estimate a convergence result easily follows. In Section 4, we describe an iterative method and show that the fix-point of the method is a solution to the non-regularized finite-difference Bingham problem. Results of numerical experiments illustrating the performance of the scheme are given in Section 5.

### 2. Finite-difference scheme

For simplicity we assume  $\bar{\Omega} = \cup_{t \in \mathcal{T}_h} t$ , where  $\mathcal{T}_h$  is the partitioning consisting of cubic (in 3D) or rectangular (in 2D) elements. All vertices of elements  $t$  form the grid domain  $\bar{\Omega}_1$  and all element

centers form the grid domain  $\Omega_2$ , denote  $\Omega_1 = \bar{\Omega}_1 \cap \Omega$ ,  $\partial\Omega_1 = \bar{\Omega}_1 \cap \partial\Omega$ . For the 2D case the grid element is shown in Fig. 1. By  $\mathbf{U}_h$  we denote the space of grid vector functions  $\mathbf{u}_h$  defined on  $\bar{\Omega}_1$  and  $P_h$  is the space of scalar grid functions defined on  $\Omega_2$ , such that  $\sum_{\mathbf{x} \in \Omega_2} p_h(\mathbf{x}) = 0$ . Both spaces are equipped with the Euclidian scalar products:  $\langle \mathbf{u}_h, \mathbf{v}_h \rangle := \sum_{\mathbf{x} \in \bar{\Omega}_1} \mathbf{u}_h(\mathbf{x}) \cdot \mathbf{v}_h(\mathbf{x})$  for  $\mathbf{u}_h, \mathbf{v}_h \in \mathbf{U}_h$  and  $\langle p_h, q_h \rangle := \sum_{\mathbf{x} \in \Omega_2} p_h(\mathbf{x}) q_h(\mathbf{x})$  for  $p_h, q_h \in P_h$ ,  $\|\cdot\|$  denotes the corresponding norms for both spaces. By  $\mathbf{Q}_h$  we denote the space of grid  $d \times d$  tensor functions  $\boldsymbol{\tau}_h$  (discrete stress and the rate of deformation tensors) defined on  $\Omega_2$ . Additionally we denote by  $\mathbf{U}_h^{int}$  the space of grid vector functions  $\mathbf{u}_h$  defined on  $\Omega_1$  (only internal nodes).

Using index notation as shown in Fig. 1 we define finite-difference scalar and vector divergence operators  $\operatorname{div}_h : \mathbf{U}_h \rightarrow P_h$  and  $\operatorname{div}_h : \mathbf{Q}_h \rightarrow \mathbf{U}_h^{int}$  through (we give formulas only for the 2D case, when the extension to the 3D case is obvious):

$$\begin{aligned}
 (\operatorname{div}_h \mathbf{u}_h)_{ij} &= \frac{u_{i+1,j+1} - u_{ij+1} + u_{i+1,j} - u_{ij}}{2h_x} \\
 &\quad + \frac{v_{i+1,j+1} - v_{i+1,j} + v_{ij+1} - v_{ij}}{2h_y}, \\
 (\operatorname{div}_h \boldsymbol{\tau}_h)_{ij} &= \left( \frac{\tau_{ij}^{11} - \tau_{i-1,j}^{11} + \tau_{ij}^{11} - \tau_{i-1,j-1}^{11}}{2h_x} \right. \\
 &\quad + \frac{\tau_{ij}^{12} - \tau_{ij-1}^{12} + \tau_{i-1,j}^{12} - \tau_{i-1,j-1}^{12}}{2h_y}, \frac{\tau_{ij}^{21} - \tau_{i-1,j}^{21} + \tau_{ij}^{21} - \tau_{i-1,j-1}^{21}}{2h_x} \\
 &\quad \left. + \frac{\tau_{ij}^{22} - \tau_{ij-1}^{22} + \tau_{i-1,j}^{22} - \tau_{i-1,j-1}^{22}}{2h_y} \right)^T.
 \end{aligned}$$

Components of the finite-difference rate of deformation tensor  $\mathbf{D}_h : \mathbf{U}_h \rightarrow \mathbf{Q}_h$  are defined as

$$\begin{aligned}
 (D_h^{11} \mathbf{u}_h)_{ij} &= \frac{u_{i+1,j+1} - u_{ij+1} + u_{i+1,j} - u_{ij}}{2h_x}, \\
 (D_h^{12} \mathbf{u}_h)_{ij} &= \frac{u_{i+1,j+1} - u_{i+1,j} + u_{ij+1} - u_{ij}}{4h_y} + \frac{v_{i+1,j+1} - v_{ij+1} + v_{i+1,j} - v_{ij}}{4h_x}, \\
 (D_h^{21} \mathbf{u}_h)_{ij} &= (D_h^{12} \mathbf{u}_h)_{ij}, \text{ the component } (D_h^{22} \mathbf{u}_h) \text{ is defined by the analog with } (D_h^{11} \mathbf{u}_h).
 \end{aligned}$$

The finite-difference gradient  $\nabla_h : P_h \rightarrow \mathbf{U}_h^{int}$  is defined as transpose to  $-\operatorname{div}_h$ . Given these discrete operators we can formally consider the finite-difference Bingham problem:

$$-\operatorname{div}_h \boldsymbol{\tau}_h + \nabla_h p_h = \mathbf{f}_h, \tag{5}$$

$$\operatorname{div}_h \mathbf{u}_h = 0, \tag{6}$$

$$\mathbf{u}_h|_{\partial\Omega_1} = \mathbf{u}_h^b,$$

where

$$\boldsymbol{\tau}_h = 2\mu \mathbf{D}_h \mathbf{u}_h + \tau_s \frac{\mathbf{D}_h \mathbf{u}_h}{|\mathbf{D}_h \mathbf{u}_h|}, \text{ if } |\mathbf{D}_h \mathbf{u}_h| \neq 0, \tag{7}$$

$$|\boldsymbol{\tau}_h| \leq \tau_s, \text{ if } |\mathbf{D}_h \mathbf{u}_h| = 0.$$

The direct application of the scheme (5)–(7) encounters the following two major problems. The Eq. (5) should be imposed only in

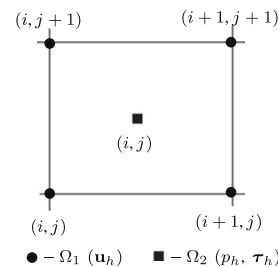


Fig. 1. A grid element.

those (*a priori* unknown!) nodes of  $\Omega_1$ , where  $|\tau_h| > \tau_s$  for the neighboring  $\Omega_2$ -nodes. This problem is overcome by defining the finite-difference solution  $\{\mathbf{u}_h, p_h, \tau_h\}$  as the limit of the sequence  $\{\mathbf{u}_h^n, p_h^n, \tau_h^n\}_{n=1,2,\dots}$  generated by a special iterative procedure. On each iteration a discrete Stokes problem is solved in the whole domain, see details in Section 4. The second problem is the well-known instability of the semi-staggered grid approximation for the Stokes problem. This instability can be characterized as follows: Besides the trivial constant vector in the kernel of the discrete gradient  $\nabla_h$  one has additional “checkerboard” mode in  $\ker(\nabla_h)$  for the 2D Stokes problem [29]. Moreover, in the 3D case the dimension of  $\ker(\nabla_h)$  is  $O(h^{-1})$  ([10], p. 244). Furthermore, restricted on the orthogonal complement of  $\ker(\nabla_h)$  in  $P_h$  the inverse of the Stokes operator is not uniformly bounded with respect to  $h$  in a natural norm, cf. Remark 7. In practice, the instability leads to non-physical pressure solutions and the poor convergence of commonly used iterative methods for solving the discrete Stokes problem. Since the Stokes problem is the particular case ( $\tau_s = 0$ ) of (5)–(7) and it appears as an auxiliary problem in the iterative procedure, see Section 4, we have to stabilize the discretization. In this paper, the stabilization is done in the spirit of the techniques well-established for finite element discretizations, see, e.g. [9,11,3,24] (below we remark on alternative approaches, see Remark 1): The discrete divergence constraint (6) is penalized

$$\operatorname{div}_h \mathbf{u}_h + G_h p_h = 0, \quad (8)$$

with a stabilization term  $G_h : P_h \rightarrow P_h$ . The operator  $G_h$  should satisfy conditions (11)–(13) and can be defined in several ways. For example, similar to the finite element method from [11] one may define  $G_h$  through

$$G_h = -\alpha h^2 \Delta_h^p, \quad (9)$$

where  $\Delta_h^p$  is the usual 5-point (7-point in 3D) approximation of the Laplace operator with the Neumann boundary conditions imposed in fictitious points. One has to chose a parameter  $\alpha$  and a “characteristic” mesh parameter  $h$ .

Another choice for  $G_h$  was suggested in [23]. Denote by  $R_h$  the space of grid scalar functions defined on  $\bar{\Omega}_1$ . Let  $\mathbf{x} \in \bar{\Omega}_1$ , and

$$\omega(\mathbf{x}) = \{\mathbf{y} \in \Omega_2 \mid |\mathbf{y} - \mathbf{x}| = |\bar{h}|/2\},$$

where  $\bar{h} = (h_x, h_y, h_z)^T$ . Define the operator  $\Pi_h : P_h \rightarrow R_h$  by

$$(\Pi_h p_h)_{ij} = |\omega(\mathbf{x}_{ij})|^{-1} \sum_{\mathbf{x}_{kl} \in \omega(\mathbf{x}_{ij})} p_{kl}.$$

The operator  $\Pi_h$  can be considered as an interpolation from  $\Omega_2$  onto  $\bar{\Omega}_1$ . Similar we define the interpolation operator  $\tilde{\Pi}_h$  from  $\bar{\Omega}_1$  onto  $\Omega_2$ . Other interpolation operators can be considered as well, in particular for non-uniform grids. We set

$$G_h := \alpha(I_h - \tilde{\Pi}_h \Pi_h), \quad (10)$$

$\alpha$  is some mesh-independent parameter,  $I_h$  is the identity operator. For uniform cubic grids ( $h_x = h_y = h_z = h$ ) we verify, see Lemma 3, that both choices in (9) and (10) satisfy conditions (11)–(13) below.

Accuracy condition: for any sufficiently smooth  $p \in L^2(\Omega)$  denote by  $(p)_h \in P_h$  the trace of  $p$  on  $\Omega_2$ , then

$$\frac{\|G_h(p)_h\|}{\|(p)_h\|} = O(h). \quad (11)$$

For  $\mathbf{x} \in \Omega_2$  denote by  $\tilde{\omega}(\mathbf{x})$  the set of neighboring nodes from  $\Omega_2$ :

$$\tilde{\omega}(\mathbf{x}) = \{\mathbf{y} \in \Omega_2 \mid |\mathbf{y} - \mathbf{x}| \leq |\bar{h}|\},$$

Stability condition: for any  $p_h \in P_h$

$$c_G \sum_{\mathbf{x} \in \Omega_2} \sum_{\mathbf{y} \in \tilde{\omega}(\mathbf{x})} (p_h(\mathbf{x}) - p_h(\mathbf{y}))^2 \leq \langle G_h p_h, p_h \rangle, \quad (12)$$

with some mesh-independent constant  $c_G > 0$ . Moreover, the operator  $G_h$  is symmetric and the estimate

$$\|G_h\| \leq C_G, \quad (13)$$

holds with another mesh-independent constant  $C_G$ . The latter assumption is less critical for the performance of the finite-difference scheme than (11) and (12), but it is helpful for building efficient linear algebraic solvers, cf. Remark 10.

**Remark 1.** A common approach of curing parasitic pressure modes problem for non-staggered approximation is to apply dissipation to the pressure field, e.g. [2,12]. This dissipation is typically introduced (sometimes implicitly) by modifying projection or velocity correction step of time-stepping algorithms. The resulting pressure dissipation term can be interpret as a discretization of a forth order differential operator and usually depends on the time step and an additional relaxation parameter. The element-wise divergence-free condition is unavoidably altered.

The present approach also introduces the pressure dissipation term. One difference is that the second-order pressure term (instead of a forth order term) was introduced. Furthermore, we avoid any time-splitting procedure, so the new term does not depend on any time-step parameter (the choice (10) avoids mesh parameter as well) making the method more attractive for steady and slowly changing in time flows. Moreover, for the new stabilized scheme we prove a rigorous stability estimate and convergence result for the case of the Stokes problem, see the next section. We are not aware of similar stability results for other non-staggered (or semi-staggered) schemes which can be found in the literature.

For the stability analysis of the next section and the solution algorithm from Section 4 we need the following “consistent” approximation of the vector Laplace operator  $\tilde{\Delta}_h : \mathbf{U}_h \rightarrow \mathbf{U}_h$ :

$$\tilde{\Delta}_h = 2\operatorname{div}_h \mathbf{D}_h - \nabla_h \operatorname{div}_h. \quad (14)$$

We note that the relation (14) leads to a different grid stencil than the common 5-point (or 7-point in 3D) approximation of  $\Delta$ . For example, with  $h_x = h_y = h_z = h$  one gets the following skew-cross 5-point (or an oblique 27-point in 3D) stencil for each velocity component:

$$2D : (\tilde{\Delta}_h u_h)_{ij} = \frac{u_{i-1,j-1} + u_{i+1,j-1} + u_{i+1,j+1} + u_{i-1,j+1} - 4u_{ij}}{2h^2}, \quad (15)$$

$$3D : (\tilde{\Delta}_h u_h)_{i,j,k} = \frac{1}{16h^2} [2(u_{i\pm 1,j\pm 1,k} + u_{i\pm 1,j,k\pm 1} + u_{i,j\pm 1,k\pm 1}) + 3u_{i\pm 1,j\pm 1,k\pm 1} - 4(u_{i\pm 1,j,k} + u_{i,j\pm 1,k} + u_{i,j,k\pm 1}) - 24u_{i,j,k}]. \quad (16)$$

### 3. Stability and error analysis for the Stokes problem

In this section, we analyze the stability of the finite-difference scheme (5),(7),(8) for the particular case of  $\tau_s = 0$ . In this case, the problem becomes linear and one can eliminate  $\tau_h$  ending up with the system of difference equations:

$$\begin{aligned} -2\operatorname{div}_h \mathbf{D}_h \mathbf{u}_h + \nabla_h p_h &= \mathbf{f}_h, \\ \operatorname{div}_h \mathbf{u}_h + G_h p_h &= 0, \\ \mathbf{u}_h|_{\partial\Omega_1} &= 0. \end{aligned} \quad (17)$$

For the sake of analysis the assume  $\Omega = (0,1)^d$  and  $h_x = h_y = h_z = h = 1/(N+1)$ . For convenience we assume that functions from  $\mathbf{U}_h$  vanish on  $\partial\Omega_1$  and introduce the discrete “energy” norm on  $\mathbf{U}_h$ :

$$\|\nabla_h \mathbf{u}_h\| := -\langle \Delta_h \mathbf{u}_h, \mathbf{u}_h \rangle^{\frac{1}{2}},$$

where  $\Delta_h$  is the common 5-point (or 7-point in 3D) approximation of the vector Laplace operator supplemented with the homogeneous Dirichlet conditions in boundary grid nodes. First we prove several technical lemmas.

We need several results for the discrete rate of deformation tensor given in the following lemma.

**Lemma 2.** *The following estimates are valid:*

$$c_A \|\mathbf{u}_h\| \leq \|\mathbf{D}_h \mathbf{u}_h\| \leq C_A \|\nabla_h \mathbf{u}_h\| \quad \forall \mathbf{u}_h \in \mathbf{U}_h, \tag{18}$$

$$|\langle p_h, \text{div}_h \mathbf{u}_h \rangle| \leq \sqrt{2} \|p_h\| \|\mathbf{D}_h \mathbf{u}_h\| \quad \forall p \in P_h, \mathbf{u}_h \in \mathbf{U}_h, \tag{19}$$

with some mesh-independent positive constants  $c_A, C_A$ .

**Proof.** The upper bound (18) is proved by the straightforward application of the triangle inequality. Further, using the summation by parts and the relation (14) for the discrete operators  $\mathbf{D}_h, \tilde{\Delta}_h$  and  $\text{div}_h$  from the previous section one verifies the identity:

$$2 \|\mathbf{D}_h \mathbf{u}_h\|^2 = \langle -\tilde{\Delta}_h \mathbf{u}_h, \mathbf{u}_h \rangle + \|\text{div}_h \mathbf{u}_h\|^2 \quad \forall \mathbf{u}_h \in \mathbf{U}_h. \tag{20}$$

This identity immediately implies the estimate (19) and the discrete Korn's type inequality:

$$\langle -\tilde{\Delta}_h \mathbf{u}_h, \mathbf{u}_h \rangle \leq 2 \|\mathbf{D}_h \mathbf{u}_h\|^2 \quad \forall \mathbf{u}_h \in \mathbf{U}_h, \tag{21}$$

It remains to show the low bound in (18). This bound follows from (21) and

$$2c_A^2 \|\mathbf{u}_h\|^2 \leq \langle -\tilde{\Delta}_h \mathbf{u}_h, \mathbf{u}_h \rangle \quad \forall \mathbf{u}_h \in \mathbf{U}_h, \tag{22}$$

In the rest of the proof we verify (22).

First we treat the case  $d = 2$ . The summation by parts gives for each velocity component

$$\langle -\tilde{\Delta}_h u_h, u_h \rangle = \sum_{t \in \mathcal{T}_h} \frac{(u_{i+1,j+1} - u_{ij})^2 + (u_{i+1,j} - u_{ij+1})^2}{2h^2}. \tag{23}$$

Now the bound in (22) (the discrete Friedreichts type inequality) follows by a standard argument from the following representation:

$$u(\mathbf{x}_{ij}) = u_{ij} = u_{i_0 j_0} + \sum_{k=0}^n (u_{i_0+k+1, j_0+k+1} - u_{i_0+k, j_0+k}) \quad \forall \mathbf{x}_{ij} \in \Omega_1,$$

with some  $n \leq ch^{-1}$  and  $\mathbf{x}_{i_0 j_0} \in \partial \Omega_1$  depending on  $\mathbf{x}_{ij}$ ; we call  $\mathbf{x}_{i_0 j_0}$  to be the basis node for  $\mathbf{x}_{ij}$ . Using  $u_{i_0 j_0} = 0$  and the Cauchy inequality one obtains

$$\begin{aligned} \|u_h\|^2 &= \sum_{\mathbf{x}_{ij} \in \Omega_1} \sum_{k=0}^n (u_{i_0+k+1, j_0+k+1} - u_{i_0+k, j_0+k}) \\ &\leq \sum_{\mathbf{x}_{ij} \in \Omega_1} ch \sum_{k=0}^n \frac{(u_{i_0+k+1, j_0+k+1} - u_{i_0+k, j_0+k})^2}{2h^2}. \end{aligned}$$

Further to show the bound in (22) one gets use of (23) and the observation that any  $\mathbf{x}_{i_0 j_0} \in \partial \Omega_1$  can be a basis node for at most  $O(h^{-1})$  inner points  $\mathbf{x}_{ij}$ .

For the 3D case one computes

$$\begin{aligned} \langle -\tilde{\Delta}_h u_h, u_h \rangle &= \sum_{t \in \mathcal{T}_h} \frac{1}{16h^2} [(a+b)^2 + (a+d)^2 + (a+c)^2 + (b \\ &\quad -c)^2 + (b-d)^2 + (c-d)^2], \end{aligned} \tag{24}$$

where

$$a = u_{i+1, j+1, k+1} - u_{ij, k}, \quad b = u_{i+1, j+1, k} - u_{ij, k+1},$$

$$c = u_{i+1, j, k+1} - u_{ij+1, k}, \quad d = u_{ij+1, k+1} - u_{i+1, j, k}.$$

Denote

$$e_{ij, k}^1 = u_{ij, k} + u_{i+1, j, k}, \quad e_{ij, k}^2 = u_{ij, k} + u_{ij+1, k}, \quad e_{ij, k}^3 = u_{ij, k} + u_{ij, k+1},$$

$$d_{ij, k}^1 = u_{ij, k} + u_{ij+1, k+1}, \quad d_{ij, k}^2 = u_{ij, k} + u_{i+1, j, k+1},$$

$$d_{ij, k}^3 = u_{ij, k} + u_{i+1, j+1, k},$$

then (24) yields

$$\begin{aligned} \langle -\tilde{\Delta}_h u_h, u_h \rangle &\geq c \sum_{t \in \mathcal{T}_h} \frac{1}{h^2} [(e_{ij+1, k+1}^1 - e_{ij, k}^1)^2 + (e_{i+1, j, k+1}^2 - e_{ij, k}^2)^2 \\ &\quad + (e_{i+1, j+1, k}^3 - e_{ij, k}^3)^2 + (d_{i+1, j, k}^1 - d_{ij, k}^1)^2 + (d_{ij+1, k}^2 \\ &\quad - d_{ij, k}^2)^2 + (d_{ij, k+1}^3 - d_{ij, k}^3)^2]. \end{aligned} \tag{25}$$

By the triangle inequality for any  $\mathbf{x}_{ij, k} \in \Omega_1$  it holds

$$|u_{ij, k}| \leq \frac{1}{2} (|e_{ij, k}^1| + |e_{i+1, j, k}^3| + |d_{ij, k}^2|). \tag{26}$$

Noting that  $e$  and  $d$  quantities vanish on the appropriate parts of boundary and using (25) and (26) we apply similar arguments as for the 2D case to prove the bound in (22) for  $d = 3$ .  $\square$

For two matrices (or discrete operators)  $A$  and  $B$  we write  $A \geq B$  iff  $A - B$  is semi-positive definite.

**Lemma 3.** *Stabilization operators defined in (9) and (10) both satisfy conditions (11)–(13).*

**Proof.** For the case (9) we get applying summation by part:

$$\langle G_h p_h, q_h \rangle = \alpha \sum_{\mathbf{x} \in \Omega_2} \sum_{\mathbf{y} \in \tilde{\omega}(\mathbf{x})} (p_h(\mathbf{x}) - p_h(\mathbf{y})) (q_h(\mathbf{x}) - q_h(\mathbf{y})).$$

Thus, conditions (11) and (13) are trivial. To show (11) we use the smoothness assumption for  $p \in L^2(\Omega)$  and Cauchy inequality:

$$\begin{aligned} \|G_h(p)_h\| &= \sup_{0 \neq q_h \in Q_h} \frac{\langle G_h(p)_h, q_h \rangle}{\|q_h\|} \\ &= \alpha \frac{\sum_{\mathbf{x} \in \Omega_2} \sum_{\mathbf{y} \in \tilde{\omega}(\mathbf{x})} (p(\mathbf{x}) - p(\mathbf{y})) (q_h(\mathbf{x}) - q_h(\mathbf{y}))}{\|q_h\|} \\ &\leq c \alpha h \sqrt{\sum_{\mathbf{x} \in \Omega_2} \sum_{\mathbf{y} \in \tilde{\omega}(\mathbf{x})} \left(\frac{p(\mathbf{x}) - p(\mathbf{y})}{h}\right)^2} \leq c_1 \alpha h \|(p)_h\|. \end{aligned}$$

Consider the case (10). Let us enumerate  $\Omega_2$ -nodes in the lexicographical order. Then one checks that the matrix  $G \in \mathbb{R}^{N^d \times N^d}$  of the operator  $G_h$  can be decomposed as

$$d = 2 : G = \alpha \frac{h^2}{32} (M \otimes L_n + L_n \otimes M),$$

$$\begin{aligned} d = 3 : G &= \alpha \frac{h^2}{192} ((M \otimes M + 9I \otimes I) \otimes L_n + L_n \otimes (M \otimes M + 9I \otimes I) \\ &\quad + M \otimes L_n \otimes M + 9I \otimes L_n \otimes I), \end{aligned}$$

where  $L_n \in \mathbb{R}^{N \times N}$  is the matrix of the one-dimensional discrete Laplacian with Neumann conditions:

$$L_n = h^{-2} \begin{pmatrix} 1 & -1 & & & \\ -1 & 2 & -1 & & \\ & \ddots & \ddots & \ddots & \\ & & -1 & 2 & -1 \\ & & & -1 & 1 \end{pmatrix},$$

and  $M \in \mathbb{R}^{N \times N}$  is the mass type matrix. For  $d = 2$  it holds  $M = \text{tridiag}(1, 6, 1)$  and for  $d = 3$  it holds  $M = \text{tridiag}(1, 4, 1)$ ,  $I$  is the identity matrix. In either case the eigenvalues of  $M$  satisfy  $0 < c \leq \lambda(M) < C$ , where  $c = 4, C = 8$  for  $d = 2$  and  $c = 2, C = 6$  for  $d = 3$ . This yields the following relation

$$c_g h^2 A_p \leq G \leq c_G h^2 A_p, \tag{27}$$

with some positive constants  $c_g$  and  $c_G$  independent of  $h$  and

$$d = 2 : A_p = I \otimes L_n + L_n \otimes I,$$

$$d = 3 : A_p = I \otimes I \otimes L_n + I \otimes L_n \otimes I + L_n \otimes I \otimes I.$$

Note that  $A_p$  is the usual 5-point (7-point in 3D) approximation of the minus Laplace operator with Neumann boundary conditions on  $\Omega_2$ . Therefore, (27) yields

$$-c_g h^2 \Delta_h^p \leq G_h \leq -c_G h^2 \Delta_h^p.$$

Now the same arguments as in the case (9) prove conditions (11)–(13).  $\square$

Further we need two auxiliary finite element spaces:  $\mathbf{U}^h \subset (H_0^1(\Omega))^d$  denotes the space of continuous vector functions  $\mathbf{u}^h$  bilinear on each grid element of  $t \in \mathcal{T}_h$  and vanishing on  $\partial\Omega$ ,  $P^h \subset L_0^2(\Omega)$  denotes the space of piecewise constant with respect to  $\mathcal{T}_h$  scalar functions  $p^h$ . We introduce two natural bijections:  $\psi_u : \mathbf{U}_h \rightarrow \mathbf{U}^h$  and  $\psi_p : P_h \rightarrow P^h$  setting

$$(\psi_u \circ \mathbf{u}_h)(\mathbf{x}) = \mathbf{u}_h(\mathbf{x}) \text{ for } \mathbf{x} \in \Omega_1 \text{ and } (\psi_p \circ p_h)(\mathbf{x}) = p_h(\mathbf{x}) \text{ for } \mathbf{x} \in \Omega_2.$$

For both spaces  $\mathbf{U}^h$  and  $P^h$  we use  $(\cdot, \cdot)$  and  $\|\cdot\|$  for the  $L^2$  scalar product and norm. These two spaces form the well known  $Q_1 - Q_0$  finite element pair for the Stokes problem, which satisfy the following ‘weak’ LBB condition [20,34,9]:

$$\sup_{\mathbf{u}^h \in \mathbf{U}^h} \frac{(p^h, \nabla \cdot \mathbf{u}^h)}{\|\nabla \mathbf{u}^h\|} \geq C_0 \|p^h\| - C_1 \left( h \sum_{\gamma} \int_{\gamma} [p^h]^2 ds \right)^{\frac{1}{2}} \quad \forall p^h \in P^h, \tag{28}$$

with some positive constants  $C_0, C_1$  independent of  $h$ . In the last term one takes the sum over all internal faces (or edges if  $d = 2$ ) of mesh elements,  $[p^h]$  denotes the jump of  $p^h$  over  $\gamma$ .

**Lemma 4.** *The following relations hold for any  $p_h \in P_h$ ,  $\mathbf{u}_h \in \mathbf{U}_h$  and  $p^h = \psi_p \circ p_h$ ,  $\mathbf{u}^h = \psi_u \circ \mathbf{u}_h$ :*

$$h^{\frac{d}{2}} \|p_h\| = \|p^h\|, \tag{29}$$

$$h^d (p_h, \operatorname{div}_h \mathbf{u}_h) = (p^h, \operatorname{div} \mathbf{u}^h), \tag{30}$$

$$h^{\frac{d}{2}} \|\nabla_h \mathbf{u}_h\| \leq C \|\nabla \mathbf{u}^h\|, \tag{31}$$

$$h^d (G_h p_h, p_h) \geq ch \sum_{\gamma} \int_{\gamma} [p^h]^2 ds, \tag{32}$$

with some constants  $C, c > 0$  independent of  $h$ .

**Proof.** Equalities (29) and (30) are easy to check by the straightforward computation. Let us check (31) for the 2D case first. To this end, consider a reference square grid element  $T := (0, 1)^2$  and a scalar grid function  $u_h$  with values  $u_h(0, 0) = a$ ,  $u_h(0, 1) = b$ ,  $u_h(1, 1) = c$ , and  $u_h(1, 0) = d$ . The corresponding bilinear function  $u^h$  on  $T$  has the form

$$u^h(x, y) = a(1-x)(1-y) + b(1-x)y + cyx + dx(1-y).$$

We may assume  $a = 0$  and  $(ih, jh) = (0, 0)$ . One computes

$$\begin{aligned} \|\nabla u^h\|_T^2 &= \frac{1}{3} [(c-b)^2 + (c-d)^2 + (c-b)b + (c-d)d + b^2 + d^2] \\ &\geq \frac{1}{6} [(c-b)^2 + (c-d)^2 + b^2 + d^2] \\ &= \frac{1}{6} [(u_{i+1,j+1} - u_{i,j+1})^2 + (u_{i+1,j+1} - u_{i+1,j})^2 + (u_{i+1,j} - u_{i,j})^2 \\ &\quad + (u_{i,j+1} - u_{i,j})^2]. \end{aligned}$$

After appropriate scaling we take the sum over all grid elements to obtain (31) with  $C = \sqrt{3}$ . Similar arguments with the reference cube prove the estimate (31) in the 3D case with  $C = \frac{3}{\sqrt{2}}$ .

We verify (32) using (12): Let  $d = 2$ , then

$$\begin{aligned} h \sum_t \int_{\gamma} [p^h]^2 ds &= h \sum_{i,j=1}^{N-1} h ((p_{i+1,j} - p_{i,j})^2 + (p_{i,j+1} - p_{i,j})^2) \\ &= -h^4 \langle \Delta_h^p p_h, p_h \rangle \leq Ch^2 \langle G_h p_h, p_h \rangle. \end{aligned}$$

Exactly the same argument proves (32) for  $d = 3$ .  $\square$

The homogeneous boundary conditions for functions in  $\mathbf{U}_h$  allow us to consider  $\operatorname{div}_h \mathbf{D}_h$  as a symmetric non-singular (due to (18)) operator on  $\mathbf{U}_h$ .

**Lemma 5.** *The following inequality holds on  $P_h$*

$$c_S I_h \leq \frac{1}{2} \operatorname{div}_h [\operatorname{div}_h \mathbf{D}_h]^{-1} \nabla_h + G_h \leq C_S I_h, \tag{33}$$

with some positive constants  $C_S, c_S$  independent of  $h$ ,  $I_h$  denotes the identity operator on  $P_h$ .

**Proof.** For arbitrary  $p_h \in P_h$  we have

$$\begin{aligned} &\left\langle \left( \frac{1}{2} \operatorname{div}_h [\operatorname{div}_h \mathbf{D}_h]^{-1} \nabla_h + G_h \right) p_h, p_h \right\rangle \\ &= \sup_{0 \neq \mathbf{u}_h \in \mathbf{U}_h} \frac{\langle p_h, \operatorname{div}_h \mathbf{u}_h \rangle^2}{\langle -2 [\operatorname{div}_h \mathbf{D}_h] \mathbf{u}_h, \mathbf{u}_h \rangle} + \langle G_h p_h, p_h \rangle \\ &= \sup_{0 \neq \mathbf{u}_h \in \mathbf{U}_h} \frac{\langle p_h, \operatorname{div}_h \mathbf{u}_h \rangle^2}{2 \|\mathbf{D}_h \mathbf{u}_h\|^2} + \langle G_h p_h, p_h \rangle. \end{aligned} \tag{34}$$

The upper bound in (33) now follows from (13) and (19). To prove the low bound we proceed with (34) using (18), (30), (31) and (32):

$$\begin{aligned} &\left\langle \left( \frac{1}{2} \operatorname{div}_h [\operatorname{div}_h \mathbf{D}_h]^{-1} \nabla_h + G_h \right) p_h, p_h \right\rangle \\ &\geq \frac{1}{2C_A} \sup_{0 \neq \mathbf{u}_h \in \mathbf{U}_h} \frac{\langle p_h, \operatorname{div}_h \mathbf{u}_h \rangle^2}{\|\nabla_h \mathbf{u}_h\|^2} + \langle G_h p_h, p_h \rangle \\ &\geq ch^d \left( \sup_{0 \neq \mathbf{u}^h \in \mathbf{U}^h} \frac{(p^h, \operatorname{div} \mathbf{u}^h)^2}{\|\nabla \mathbf{u}^h\|^2} + h \sum_{\gamma} \int_{\gamma} [p^h]^2 ds \right), \end{aligned}$$

with some mesh-independent  $c > 0$ . Now (28) and (29) give

$$\langle (\operatorname{div}_h [\operatorname{div}_h \mathbf{D}_h]^{-1} \nabla_h + G_h) p_h, p_h \rangle \geq c \|p_h\|^2,$$

with some mesh-independent  $c > 0$ .  $\square$

On the product space  $\mathbf{U}_h \times P_h$  we introduce the norm

$$\|(\mathbf{u}_h, p_h)\| = h^{\frac{d}{2}} (\|\mathbf{u}_h\|_{\mathbf{U}_h}^2 + \|p_h\|_{P_h}^2)^{\frac{1}{2}} := h^{\frac{d}{2}} (\|\mathbf{D}_h \mathbf{u}_h\|^2 + \|p_h\|^2)^{\frac{1}{2}}.$$

The  $h^{\frac{d}{2}}$  scaling factor is introduced to make the norm consistent with a continuous norm.

Consider the finite difference Stokes operator on  $\mathbf{U}_h \times P_h$ :

$$\mathcal{A}_h := \begin{pmatrix} -2 \operatorname{div}_h \mathbf{D}_h & \nabla_h \\ -\operatorname{div}_h & -G_h \end{pmatrix}.$$

The following stability estimate is the main result for the Stokes problem (42).

**Theorem 6.** *The discrete Stokes operator satisfies*

$$\|(\mathcal{A}_h^{-1})\| \leq C, \tag{35}$$

with the constant  $C = \left(1 + \frac{1}{\sqrt{2}}\right)^2 \max\{(2c_A)^{-1}, c_S^{-1}\}$  independent of  $h$ .

**Proof.** Denote  $L_h = 2 \operatorname{div}_h \mathbf{D}_h$ ,  $S_h := \operatorname{div}_h L_h^{-1} \nabla_h + G_h$  and consider the following factorization

$$\mathcal{A}_h := \begin{pmatrix} I_h & 0 \\ L_h^{-1} \operatorname{div}_h & I_h \end{pmatrix} \begin{pmatrix} -L_h & 0 \\ 0 & -S_h \end{pmatrix} \begin{pmatrix} I_h & -L_h^{-1} \nabla_h \\ 0 & I_h \end{pmatrix}.$$

Thus, for the inverse operator we have

$$\mathcal{A}_h^{-1} := \begin{pmatrix} I_h & L_h^{-1} \nabla_h \\ 0 & I_h \end{pmatrix} \begin{pmatrix} -L_h^{-1} & 0 \\ 0 & -S_h^{-1} \end{pmatrix} \begin{pmatrix} I_h & 0 \\ -L_h^{-1} \operatorname{div}_h & I_h \end{pmatrix}. \tag{36}$$

Let us estimate each factor on the right-hand side of (36) separately. For the first term we have

$$\left\| \begin{pmatrix} I_h & L_h^{-1} \nabla_h \\ 0 & I_h \end{pmatrix} \right\| \leq 1 + \|L_h^{-1} \nabla_h\|_{P_h \rightarrow \mathbf{U}_h}. \tag{37}$$

For arbitrary  $p_h \in P_h$  consider  $\mathbf{u}_h = L_h^{-1} \nabla_h p_h$ , then we get

$$\begin{aligned} \|\mathbf{u}_h\|_{\mathbf{U}_h}^2 &= -\frac{1}{2} \langle L_h \mathbf{u}_h, \mathbf{u}_h \rangle = -\frac{1}{2} \langle \nabla_h p_h, \mathbf{u}_h \rangle = \frac{1}{2} \langle p_h, \operatorname{div}_h \mathbf{u}_h \rangle \\ &\leq \frac{1}{\sqrt{2}} \|p_h\| \|\mathbf{D}_h \mathbf{u}_h\|. \end{aligned}$$

Therefore

$$\|L_h^{-1} \nabla_h\|_{P_h \rightarrow \mathbf{U}_h} \leq \frac{1}{\sqrt{2}}. \tag{38}$$

The third term on the right-hand side of (36) is adjoint to the first one and hence enjoys the same estimate. For the second factor we have

$$\left\| \begin{pmatrix} -L_h^{-1} & 0 \\ 0 & -S_h^{-1} \end{pmatrix} \right\| \leq \max\{\|L_h^{-1}\|_{\mathbf{U}_h \rightarrow \mathbf{U}_h}, \|S_h^{-1}\|_{P_h \rightarrow P_h}\}. \tag{39}$$

For arbitrary  $\mathbf{v}_h \in \mathbf{U}_h$  and  $\mathbf{u}_h = -L_h^{-1} \mathbf{v}_h$  we get

$$\begin{aligned} \|\mathbf{u}_h\|_{\mathbf{U}_h}^2 &= -\frac{1}{2} \langle L_h \mathbf{u}_h, \mathbf{u}_h \rangle = \frac{1}{2} \langle \mathbf{v}_h, \mathbf{u}_h \rangle \leq \frac{1}{2} \|\mathbf{u}_h\| \|\mathbf{v}_h\| \\ &\leq \frac{1}{2c_A} \|\mathbf{D}_h \mathbf{u}_h\| \|\mathbf{D}_h \mathbf{v}_h\|. \end{aligned}$$

This yields

$$\|L_h^{-1}\|_{\mathbf{U}_h \rightarrow \mathbf{U}_h} \leq (2c_A)^{-1}. \tag{40}$$

Finally, since  $S_h$  is symmetric the low bound in (33) implies

$$\|S_h^{-1}\|_{P_h \rightarrow P_h} = \lambda_{\min}^{-1}(S_h) \leq c_S^{-1}. \tag{41}$$

Now (36) and estimates (36)–(41) give

$$\|\mathcal{A}_h^{-1}\| \leq \left(1 + \frac{1}{\sqrt{2}}\right)^2 \max\{(2c_A)^{-1}, c_S^{-1}\}. \quad \square$$

The convergence result follows immediately from the theorem and approximation properties of the discrete operators:

**Corollary 1.** Assume that the solution  $\{\mathbf{u}, p\}$  of the Stokes problem:

$$\begin{aligned} -\Delta \mathbf{u} + \nabla p &= \mathbf{f} \text{ on } \Omega, \\ \operatorname{div} \mathbf{u} &= 0 \text{ on } \Omega, \\ \mathbf{u} &= 0 \text{ on } \partial\Omega \end{aligned}$$

is sufficiently smooth and  $\{\mathbf{u}_h, p_h\}$  is the solution of the discrete Stokes problem (17) with  $\mathbf{f}_h = (\mathbf{f})_h$ , then

$$\|(\mathbf{u})_h - \mathbf{u}_h, (p)_h - p_h\| = O(h).$$

Note that we proved the first order convergence for velocity in the ‘gradient’ norm. Numerical experiments show the (expected) second order of convergence for the velocity in the  $L^2$  norm. It is also straightforward to conclude from (7) for  $\tau_s = 0$  that one has the first order convergence in the  $L^2$ -norm for the stress tensor.

**Remark 7.** Assume that the stabilization term  $G_h$  is not added to the discrete divergence constraint, then the non-trivial kernel of  $\nabla_h$  makes the matrix  $S_h$  singular and thus  $\mathcal{A}_h^{-1}$  is not well-defined. Moreover, in this case the minimal nonzero eigenvalue of  $S_h$  tends to zero as  $h \rightarrow 0$ . Indeed, in [7] such an  $h$ -dependence was shown for the case of  $Q_1 - Q_0$  finite element discretization. Due to the close relation between this discretization and the finite-difference method, see Lemma 4, the same  $h$ -dependence of  $\lambda(S_h)$  should be expected. Therefore, factorization (36) shows that in the case of  $G_h \equiv 0$  the norm of  $\mathcal{A}_h^{-1}$  cannot be uniformly bounded for  $h \rightarrow 0$  even on  $\mathbf{U}_h \times (\ker \nabla_h)^\perp$ .

**Remark 8.** Finally, we remark on the following discrete Stokes problem:

$$\begin{aligned} -\Delta_h \mathbf{u}_h + \nabla_h p_h &= \mathbf{f}_h, \\ \operatorname{div}_h \mathbf{u}_h + G_h p_h &= 0, \\ \mathbf{u}_h|_{\partial\Omega_1} &= 0. \end{aligned} \tag{42}$$

Unlike the continuous case, the discrete Stokes problem (42) is not equivalent to (17). We briefly discuss (42) for the following reasons. The algorithm for the Bingham problem from the next section requires the solution of the discrete Stokes problem on every iteration. Commonly used block iterative methods for the Stokes problem need an approximation to the velocity sub-matrix inverse, cf. remark (10). For the approximation of  $\Delta_h^{-1}$  many efficient methods such as the multigrid algorithm are available. At the same time we found that the performance of a standard multigrid for solving  $[\operatorname{div}_h \mathbf{D}_h] \mathbf{u}_h = \mathbf{g}_h$  may be not satisfactory. That is why we prefer solving (42) instead of (17) and introduce appropriate correction terms to the right-hand side. Furthermore, if one uses the semi-staggered scheme for Newtonian flows, then (42) may be considered as a more natural way to discretize the Stokes problem. The stability and convergence results similar to the Theorem 6 and Corollary 1 hold also for the system (42) with a slightly different product norm on  $\mathbf{U}_h \times P_h$ :

$$\|[\mathbf{u}_h, p_h]\| = h^{\frac{d}{2}} (\|\mathbf{u}_h\|_{\mathbf{U}_h}^2 + \|p_h\|_{P_h}^2)^{\frac{1}{2}} := h^{\frac{d}{2}} (\|\nabla_h \mathbf{u}_h\|^2 + \|p_h\|^2)^{\frac{1}{2}},$$

instead of the  $\|\cdot, \cdot\|$  norm. The proof can be adjusted in an obvious way.

#### 4. Iterative method

The iterative method we use is motivated by the variational inequality and augmented Lagrangian approach by Lions, Glowinski and others, see [14,18,19]. First we recall the idea of the approach for the continuous problem. Further we adapt it for the particular discretization suggested in Section 2. To this end, consider the following functional on  $\mathbf{V} = \{\mathbf{v} \in (H_0^1(\Omega))^d \mid \operatorname{div} \mathbf{v} = 0\}$

$$J(\mathbf{v}) = \mu \int_{\Omega} |\mathbf{D}(\mathbf{v})|^2 \, d\mathbf{x} + \tau_s \int_{\Omega} |\mathbf{D}(\mathbf{v})| \, d\mathbf{x} - 2 \int_{\Omega} \mathbf{f} \cdot \mathbf{v} \, d\mathbf{x}.$$

The velocity solution  $\mathbf{u}$  of the Bingham problem (1)–(4) minimizes  $J$  on  $\mathbf{V}$  [14]:

$$\mathbf{u} = \arg \min_{\mathbf{v} \in \mathbf{V}} J(\mathbf{v}).$$

To overcome the problem of non-differentiability of  $\int_{\Omega} |\mathbf{D}(\mathbf{v})| \, d\mathbf{x}$  it was suggested in [18] to introduce the new variable  $\gamma = \mathbf{D}(\mathbf{v}) \in \mathbf{Q}$ , where  $\mathbf{Q} = \{\mathbf{q} \mid \mathbf{q} \in (L^2(\Omega))^{n \times n}, \mathbf{q}^T = \mathbf{q}\}$  and consider the following Lagrangian

$$\begin{aligned} \mathcal{L}(\mathbf{v}; \gamma; \tau) &= \mu \int_{\Omega} |\gamma|^2 \, d\mathbf{x} + \tau_s \int_{\Omega} |\gamma| \, d\mathbf{x} \\ &\quad + \int_{\Omega} (\mathbf{D}(\mathbf{v}) - \gamma) : \tau \, d\mathbf{x} - 2 \int_{\Omega} \mathbf{f} \cdot \mathbf{v} \, d\mathbf{x}. \end{aligned}$$

Thus one looks for the solution of the Bingham problem  $\{\mathbf{u}, \gamma, \tau\}$  as the saddle point of  $\mathcal{L}$ :

$$\{\mathbf{u}, \gamma, \tau\} = \arg \min_{\mu \in Q} \max_{\xi \in Q} \mathcal{L}(\mathbf{v}; \mu; \xi).$$

For a given  $\xi$  and  $\mu$  the Lagrangian  $\mathcal{L}$  is not coercive with respect to  $\mathbf{v}$ . To make it coercive one may consider the augmented Lagrangian  $\mathcal{L}_r : \mathbf{V} \times Q \times Q \rightarrow \mathbb{R}$

$$\mathcal{L}_r(\mathbf{v}; \gamma; \tau) = \mathcal{L}(\mathbf{v}; \gamma; \tau) + r \int_{\Omega} |\mathbf{D}(\mathbf{v}) - \gamma|^2 dx, \quad r \geq 0.$$

with some penalty parameter  $r > 0$ . For finding the saddle point of  $\mathcal{L}_r$  one may use the Uzawa type algorithm suggested in [19]: For given initial guess  $\gamma^0, \tau^0$  and  $n = 0, 1, 2, \dots$

1. Find  $\mathbf{u}^{n+1} \in \mathbf{V}$  such that  $\mathcal{L}_r(\mathbf{u}^{n+1}; \gamma^n; \tau^n) \leq \mathcal{L}_r(\mathbf{v}; \gamma^n; \tau^n) \quad \forall \mathbf{v} \in \mathbf{U}$ .
2. Find  $\gamma^{n+1}$  such that  $\mathcal{L}_r(\mathbf{u}^{n+1}; \gamma^{n+1}; \tau^n) \leq \mathcal{L}_r(\mathbf{u}^{n+1}; \mu; \tau^n) \quad \forall \mu \in Q$ .
3. Set  $\tau^{n+1} := \tau^n + 2r(\mathbf{D}(\mathbf{u}^{n+1}) - \gamma^{n+1})$ . It was proved in [19] that the algorithm converges for all  $r > 0$ .

Based on the above Uzawa type algorithm for the continuous Bingham problem we deduce below iterative method for solving the following discrete Bingham problem:

$$-\mathbf{div}_h \tau_h + \nabla_h p_h = \mathbf{f}_h, \tag{43}$$

$$\mathbf{div}_h \mathbf{u}_h + G_h p_h = 0, \tag{44}$$

$$\mathbf{u}_h|_{\partial\Omega_1} = \mathbf{u}_h^b, \tag{45}$$

where

$$\tau_h = 2\mu \mathbf{D}_h \mathbf{u}_h + \tau_s \frac{\mathbf{D}_h \mathbf{u}_h}{|\mathbf{D}_h \mathbf{u}_h|}, \text{ if } |\mathbf{D}_h \mathbf{u}_h| \neq 0, \tag{46}$$

$$|\tau_h| \leq \tau_s, \text{ if } |\mathbf{D}_h \mathbf{u}_h| = 0.$$

The iterative method for solving problem (43)–(46) reads:

Step 1: Given  $\gamma_h^n \in Q_h$  and  $\tau_h^n \in Q_h$  find the solution  $\mathbf{u}_h^{n+1}, p_h^{n+1}$  of the discrete Stokes problem:

$$-r \Delta_h \mathbf{u}_h^{n+1} + \nabla_h p_h^{n+1} = \mathbf{div}_h(\tau_h^n - 2r\gamma_h^n) - r(\Delta_h - \tilde{\Delta}_h)\mathbf{u}_h^n + r\nabla_h G_h p_h^n + \mathbf{f}_h, \tag{47}$$

$$\mathbf{div}_h \mathbf{u}_h^{n+1} + G_h p_h^{n+1} = 0, \tag{48}$$

$$\mathbf{u}_h|_{\partial\Omega_1} = \mathbf{u}_h^b.$$

Step 2: Compute  $\gamma_h^{n+1} \in Q_h$  via

$$\gamma_h^{n+1} := \begin{cases} 0, & \text{if } |\tau_h^n + 2r\mathbf{D}_h \mathbf{u}_h^{n+1}| < \tau_s, \\ \left(1 - \frac{\tau_s}{|\tau_h^n + 2r\mathbf{D}_h \mathbf{u}_h^{n+1}|}\right) \frac{\tau_h^n + 2r\mathbf{D}_h \mathbf{u}_h^{n+1}}{2(r+\mu)}, & \text{otherwise.} \end{cases} \tag{49}$$

Step 3: Set

$$\tau_h^{n+1} := \tau_h^n + 2r(\mathbf{D}_h \mathbf{u}_h^{n+1} - \gamma_h^{n+1}). \tag{50}$$

If  $\|\tau^{n+1} - \tau^n\| > \epsilon$  for some  $\epsilon > 0$  proceed with step 1.

Note that steps 2 and 3 of the algorithm amount to explicit node-by-node calculations. On the step 1 one needs to solve the discrete Stokes problem. Nowadays many iterative methods are available to solve this problem efficiently, see, e.g. [4,30]. Proving the convergence of the method (47)–(50) is beyond the scope of this paper. The lemma below demonstrates that the fix point of (47)–(50) is the solution to the finite-difference Bingham problem (43)–(46)

**Lemma 9.** Assume  $\|\tau_h^{n-1} - \tau_h^n\| = 0$  for all  $n \geq N$ . Then the triple  $\mathbf{v}_h^{n+1}, p_h^{n+1}, \tau_h^{n+1}$  solves (43)–(46). Moreover, if (43)–(46) has a unique solution then  $\mathbf{v}_h^{n+1}, p_h^{n+1}$ , and  $\tau_h^{n+1}$  do not depend on the choice of the penalty parameter  $r > 0$ .

**Proof.** The equality  $\|\tau_h^{n-1} - \tau_h^n\| = 0$  and (50) imply

$$\mathbf{D}_h \mathbf{v}_h^n = \gamma_h^n. \tag{51}$$

Thanks to the condition (14) and relations (51) we can rewrite the Eqs. (47) and (48) in the following way:

$$-\mathbf{div}_h \tau_h^n + \nabla_h p_h^{n+1} = \mathbf{f}_h - r \Delta_h(\mathbf{v}_h^n - \mathbf{v}_h^{n+1}) + r \nabla_h G_h(p_h^n - p_h^{n+1}), \tag{52}$$

$$\mathbf{div}_h \mathbf{v}_h^{n+1} + G_h p_h^{n+1} = 0. \tag{53}$$

Introduce the notation

$$\mathbf{T}_h = \tau_h^n + 2r\mathbf{D}_h \mathbf{v}_h^{n+1}. \tag{54}$$

Taking (51) into account (for  $n + 1$  instead of  $n$ ) we get from (49)

$$\mathbf{D}_h(\mathbf{v}_h^{n+1}) := \begin{cases} 0, & \text{if } |\mathbf{T}_h| < \tau_s, \\ \left(1 - \frac{\tau_s}{|\mathbf{T}_h|}\right) \frac{\mathbf{T}_h}{2(r+\mu)}, & \text{otherwise.} \end{cases}$$

This relation is equivalent to

$$\mathbf{T}_h = 2(\mu + r)\mathbf{D}_h \mathbf{v}_h^{n+1} + \tau_s \frac{\mathbf{D}_h \mathbf{v}_h^{n+1}}{|\mathbf{D}_h \mathbf{v}_h^{n+1}|}, \text{ if } |\mathbf{D}_h \mathbf{v}_h^{n+1}| \neq 0,$$

$$|\mathbf{T}_h| \leq \tau_s, \text{ if } |\mathbf{D}_h \mathbf{v}_h^{n+1}| = 0.$$

Due to (54) we obtain

$$\tau_h^n = 2\mu \mathbf{D}_h \mathbf{v}_h^{n+1} + \tau_s \frac{\mathbf{D}_h \mathbf{v}_h^{n+1}}{|\mathbf{D}_h \mathbf{v}_h^{n+1}|}, \text{ if } |\mathbf{D}_h \mathbf{v}_h^{n+1}| \neq 0, \tag{55}$$

$$|\tau_h^n| \leq \tau_s, \text{ if } |\mathbf{D}_h \mathbf{v}_h^{n+1}| = 0.$$

Since  $\tau_h^{n-1} = \tau_h^n$  the relation (55) yields  $\mathbf{D}_h \mathbf{v}_h^n = \mathbf{D}_h \mathbf{v}_h^{n+1}$ . Hence the discrete Korn's inequality (21) and (22) imply  $\mathbf{v}_h^n = \mathbf{v}_h^{n+1}$ . Thus, we get from (52) and (53)

$$-\mathbf{div}_h \tau_h^n + \nabla_h p_h^{n+1} = \mathbf{f}_h, \tag{56}$$

$$\mathbf{div}_h \mathbf{v}_h^{n+1} + G_h p_h^{n+1} = 0, \tag{57}$$

Therefore, the triple  $\mathbf{v}_h^{n+1}, p_h^{n+1}, \tau_h^n$  satisfies the system of finite-difference Eqs. (56) and (57), and constitutive relation (55), which is equivalent to (43)–(46). Since the system (43)–(46) does not depend on the parameter  $r$ , the uniqueness assumption ensures that the fix point of the iterative method (47)–(50) is independent of  $r$ .  $\square$

**Remark 10.** The most computationally expensive part of the algorithm is solving the discrete Stokes problem on step 1. The stability results of the previous section allows a variety of iterative methods to be used for this purpose. In our numerical experiments we use preconditioned BiCGstab algorithm with the following block-triangular preconditioner from [16]:

$$\tilde{\mathcal{A}}_h := \begin{pmatrix} \tilde{\Delta}_h^{-1} & 0 \\ -\mathbf{div}_h & \tilde{S}_h \end{pmatrix},$$

where  $\tilde{\Delta}_h$  is a preconditioner for the discrete Laplace operator and  $\tilde{S}_h$  is a preconditioner for the pressure Schur complement matrix  $S_h = \mathbf{div}_h \Delta_h^{-1} \nabla_h + G_h$ . In our experiments we define  $\tilde{\Delta}_h$  as one V(3,3) cycle of the standard multigrid method, providing a spectral equivalent preconditioner of the optimal complexity [21]. Due to estimates (33), which also holds with  $2\mathbf{div}_h \mathbf{D}_h$  replaced by  $\Delta_h$ , the simple choice  $\tilde{S}_h := I_h$  gives an effective preconditioner for  $S_h$ . Finally we note that including inertia terms to the Bingham problem would lead to the Oseen type problem on step 1, which can be treated within the same framework [16,26].

5. Numerical results

5.1. The Stokes problem

We start with verifying convergence results for the finite-difference scheme applied to the Stokes problem. In this case it is easy to prescribe an analytical solution. The following example from [6] was used in 2D:

$$\mathbf{u} = \begin{cases} \frac{r_2}{2\pi} \frac{e^{r_2 y}}{(e^{r_2} - 1)} \sin\left(\frac{2\pi(e^{r_2 y} - 1)}{e^{r_2} - 1}\right) \left(1 - \cos\left(\frac{2\pi(e^{r_1 x} - 1)}{e^{r_1} - 1}\right)\right), \\ -\frac{r_1}{2\pi} \frac{e^{r_1 x}}{(e^{r_1} - 1)} \sin\left(\frac{2\pi(e^{r_1 x} - 1)}{e^{r_1} - 1}\right) \left(1 - \cos\left(\frac{2\pi(e^{r_2 y} - 1)}{e^{r_2} - 1}\right)\right), \end{cases} \quad (58)$$

$$p = r_1 r_2 \sin\left(\frac{2\pi(e^{r_1 x} - 1)}{e^{r_1} - 1}\right) \sin\left(\frac{2\pi(e^{r_2 y} - 1)}{e^{r_2} - 1}\right) \times \frac{e^{r_1 x} e^{r_2 y}}{(e^{r_1} - 1)(e^{r_2} - 1)}, \quad (59)$$

with  $r_1 = 4, r_2 = 0.1$ . The solution (58) and (59) is illustrated in Fig. 2, it simulates a rotating cavity vortex, whose center has coordinates  $(x_0, y_0)$ ,  $x_0 = 1/r_1 \log((\exp(r_1) + 1)/2) \approx 0.842$ ,  $y_0 = 1/r_2 \log((\exp(r_2) + 1)/2) \approx 0.512$  and  $\max_{\Omega} |\mathbf{u}| \approx 1$ . Hence a boundary layer occurs near the right part of the boundary.

For the 3D problem we use the example from [9]:

$$\mathbf{u} = \begin{cases} x + x^2 + xy + x^3 y, \\ y + xy + y^2 + x^2 y^2, \\ -2z - 3xz - 3yz - 5x^2 yz, \end{cases} \quad (60)$$

$$p = xyz + x^3 y^3 z - 5./32.$$

Table 1 shows the discrete  $L_2$  norms of the errors in the velocity and pressure with the analytical solutions (58)–(60). The right column shows the maximum number of iteration of the preconditioned BiCGstab method, cf. Remark 10, which is needed to reduce the residual of the Stokes problem (47) and (48) by the factor  $10^{-9}$ . The second order of convergence is observed for the velocity and almost the second order for the pressure, although only the  $O(h)$  theoretical bound was proved in the latter case. The performance of the iterative method for the discrete Stokes problem was predicted to be independent of the mesh size. This is confirmed by the numerical results. In this numerical experiment and further on we use the stabilization matrix  $G_h$  from (10) with  $\alpha = 0.25$ .

5.2. The Bingham problem

Observing the optimal convergence results for the Stokes problem we perform numerical experiments for the Bingham problem, both in 2D and 3D cases. For all tests we use the algorithm (47)–(50) with  $r = 4$  and the stopping criteria  $\|\mathbf{D}_h \mathbf{u}_h^{n+1} - \mathbf{u}_h^{n+1}\| \leq 10^{-5}$

or a maximum of 1000 iterations. The Stokes problem (47) and (48) is solved iteratively with  $\mathbf{u}_h^n, p^n$  as an initial guess, these iterations are performed until the residual decreases at least by the factor  $10^{-3}$ . In all experiments we set  $\mu = 1$  and vary  $\tau_s$ . We note that the convergence of the algorithm (47)–(50) appears to be rather slow and getting worse with the increase of  $\tau_s$  in all tests considered below, see, e.g. Table 2.

5.2.1. Analytical test

Unlike the Stoke case, not a lot of reasonable analytical solutions are known for the Bingham problem. One is the flow between two planes:

$$u = \begin{cases} \frac{1}{8}(1 - 2\tau_s)^2, & \text{if } \frac{1}{2} - \tau_s \leq y \leq \frac{1}{2} + \tau_s, \\ \frac{1}{8}[(1 - 2\tau_s)^2 - (1 - 2\tau_s - 2y)^2], & \text{if } 0 \leq y < \frac{1}{2} - \tau_s, \\ \frac{1}{8}[(1 - 2\tau_s)^2 - (2y - 2\tau_s - 1)^2], & \text{if } 1 > y > \frac{1}{2} + \tau_s, \end{cases} \quad (61)$$

$$v = w = 0,$$

$$p = -x.$$

The rigid region consists of a constantly moving kernel for  $\frac{1}{2} - \tau_s \leq y \leq \frac{1}{2} + \tau_s$ . The yield stress  $\tau_s = 0.5$  is the critical value, when the flow region disappears. The solution can be considered in the 3D as well as in the 2D case.

For the computation domain we consider the unit cube  $(0, 1)^d$ ,  $d = 2, 3$ . The boundary conditions in (47) are prescribed based on (61). In this setting Table 2 shows the convergence of the difference solution for the several values of  $\tau_s$ :  $err_u$ ,  $err_p$ , and  $err_t$  denote the  $L^2$ -norms for velocity, pressure and stress tensor, respectively. The norm of the error in pressure and the stress tensor was measured only in the flow region. Although some convergence deterioration can be noted compared to the Stokes case, the order of convergence is largely the same. In 2D the performance of the scheme was found to be similar.

Table 1  
Convergence of the FD solution and iteration number for the Stokes equations.

$h$	$\ (\mathbf{u})_h - \mathbf{v}_h\ $	$\log_2 \frac{\ (\mathbf{u})_h - \mathbf{v}_h\ }{\ (\mathbf{u})_{2h} - \mathbf{v}_{2h}\ }$	$\ (p)_h - p_h\ $	$\log_2 \frac{\ (p)_h - p_h\ }{\ (p)_{2h} - p_{2h}\ }$	#Iter
2D test					
$\frac{1}{32}$	6.21e-3	2.03	1.14e-1	1.95	15
$\frac{1}{64}$	1.52e-3	2.00	2.96e-2	1.81	17
$\frac{1}{128}$	3.79e-4	2.01	8.46e-3	1.72	17
$\frac{1}{256}$	9.44e-5		2.57e-3		17
3D test					
$\frac{1}{16}$	2.544e-4	1.95	8.141e-3	1.77	30
$\frac{1}{32}$	6.537e-5	1.99	2.393e-3	1.82	30
$\frac{1}{64}$	1.654e-5		6.776e-4		31

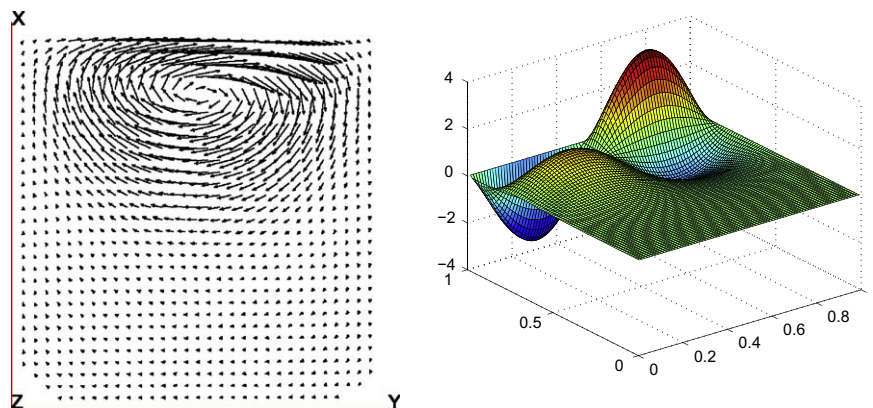
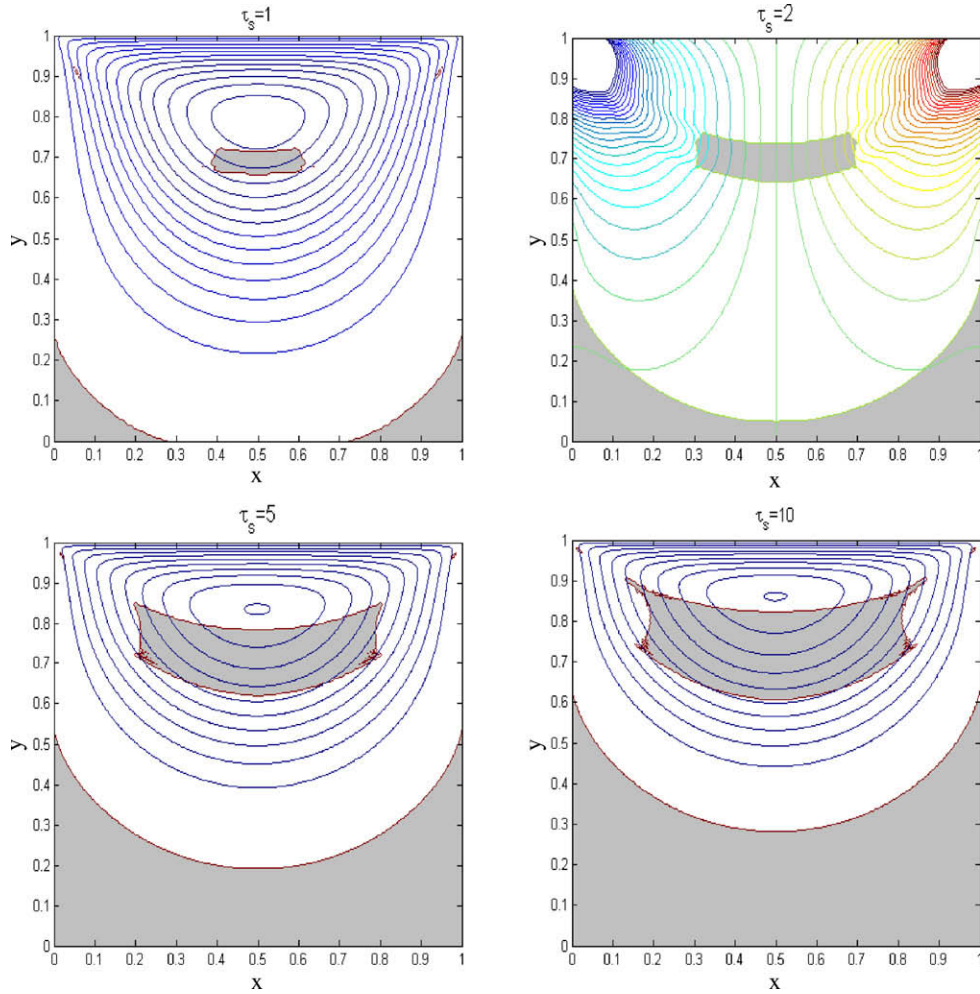


Fig. 2. Velocity and pressure from (58) and (59).

**Table 2**  
Convergence of the FD solution and iteration number for the 3D Bingham flow (61).

h	err <sub>u</sub>	err <sub>p</sub>	err <sub>τ</sub>	#Iter	err <sub>u</sub>	err <sub>p</sub>	err <sub>τ</sub>	#Iter
	$\tau_s = 0$				$\tau_s = 0.1$			
$\frac{1}{16}$	2.63e-4	5.19e-3	3.37e-3	7	2.98e-4	1.37e-2	5.79e-3	44
$\frac{1}{32}$	6.69e-5	1.50e-3	1.103e-3	7	7.37e-5	4.56e-3	2.57e-3	33
$\frac{1}{64}$	1.65e-5	3.84e-4	3.726e-4	7	2.01e-5	2.19e-4	1.63e-3	53
	$\tau_s = 0.2$				$\tau_s = 0.3$			
$\frac{1}{16}$	2.91e-4	2.19e-2	9.56e-3	56	2.85e-4	3.86e-2	1.07e-3	153
$\frac{1}{32}$	7.72e-5	8.46e-3	4.88e-3	77	8.02e-5	1.22e-2	4.10e-3	156
$\frac{1}{64}$	1.99e-5	2.46e-3	1.55e-3	78	1.97e-5	4.01e-3	2.37e-3	138



**Fig. 3.** Stream-function isolines, isobars and rigid zones, 2D problem. Upper pictures:  $\tau_s = 1$  and  $\tau_s = 2$ ; bottom:  $\tau_s = 5$  and  $\tau_s = 10$ .

5.2.2. Driven cavity test

The next test is the two-dimensional and three-dimensional driven-cavity problem:  $\Omega = (0, 1)^d$ ,  $\mathbf{f} = 0$ , with  $\mathbf{u}(\mathbf{x})|_{z=1} = (1, 0, 0)$  and homogeneous Dirichlet boundary conditions on the rest part of the boundary. The solution has a non-physical singular behavior in the upper corners, however, the problem serves as a standard benchmark for incompressible CFD codes.

In Figs. 3 and 5 we show the stream-function isolines, isobars and rigid zones for different values of  $\tau_s$  ( $h = \frac{1}{256}$ ). For finding rigid zones we use the following criteria:  $|\tau_h| \leq (1 + \varepsilon)\tau_s$ , with an ad hoc  $\varepsilon = 10^{-3}$  which is introduced to remove some oscillations of the modula of the discrete stress tensor near the critical value  $\tau_s$ . For a better resolution of rigid zones one likely needs to refine adaptively the mesh near the interface between solid and fluid regions.

Not so many quantitative results for the Bingham driven cavity flow can be found in the literature, so a somewhat limited comparison with results from other papers can be made. Moreover, we have not found any other results for the 3D Bingham driven cavity flow except the paper [15], where the problem with periodic conditions in  $y$ -direction was studied, thus the solution computed in [15] is essentially two-dimensional. With these reservations we remark that the shape and the position of the rigid zones in the 2D case are in a good agreement with the results from [15,22,31] computed with finite element approximations. The rigid regions are growing when the stress yield increases. The results with stabilized semi-staggered grid for a regularized cavity problem (not shown here) are also close to those obtain with the MAC-type scheme in [23]. We note some overlap of the center rigid zone and the

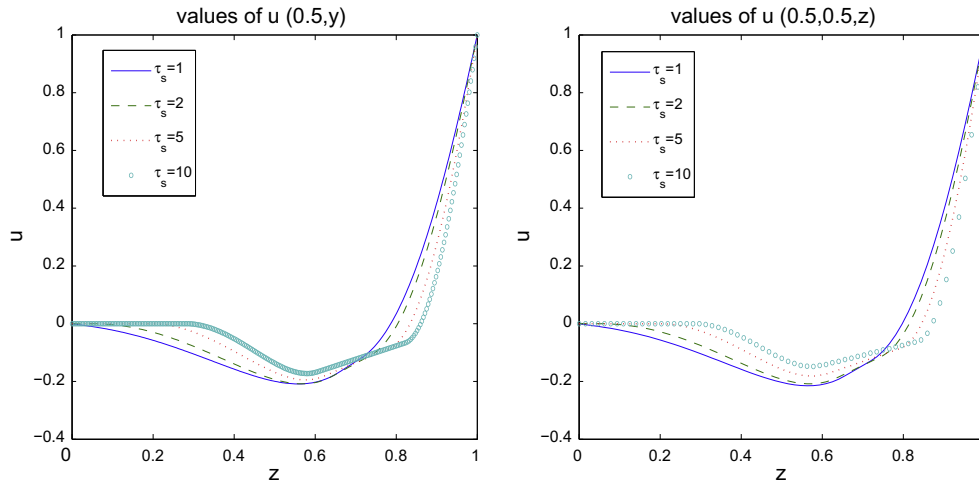


Fig. 4. Horizontal velocity profiles. Left:  $u(0.5,y)$  (2D cavity); Right:  $u(0.5,0,5,z)$  (3D cavity).

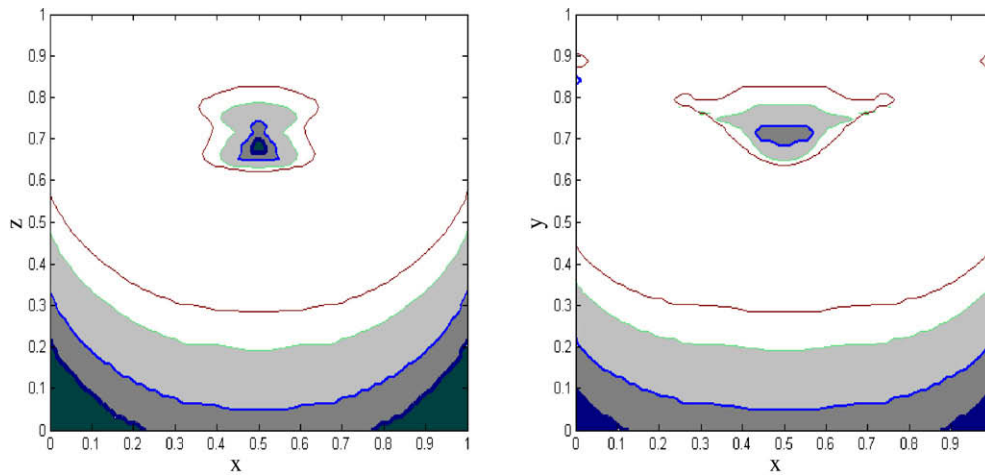


Fig. 5. Rigid zones for the 3D cavity with  $\tau_s = 1, 2, 5, 10$ . Left:  $xz$ -plane for  $y = 0.5$ ; Right:  $yz$ -plane for  $x = 0.5$ .

**Table 3**  
Position of the center and the vortex intensity for the 2D driven cavity.

$\tau_s$	0	1	2	5	10
$\phi_{\min}$	-0.09980	-0.08978	-0.08233	-0.07881	-0.05697
$x_m$	0.50	0.50	0.50	0.50	0.50
$y_m$	0.7646	0.7881	0.8057	0.8350	0.8623

stream-function isolines. This phenomena can be also noted in the result shown in other papers: [13,15,22,35].

Fig. 4 shows the velocity  $x$ -component profiles for  $x = 0.5$ . These profiles are in a very good agreement with those found in [35] with P1/P1 stabilized elements. Other quantities of interest are the minimum value of the stream function (vortex intensity) and the coordinates of the vortex center. The computed values of these quantities for various  $\tau_s$  are given in Table 3. For the Newtonian flow ( $\tau_s = 0$ ) the present values are very close to the reference values  $\phi_{\min} = -0.10007627$ ,  $y_m = 0,7644162$  computed in [1,8] with higher order methods. As the stress yield increases the vortex center travels to the upper lid and its intensity decreases. The same trend with similar values of the vortex intensity and position were achieved in [22] using a finite element method. The computed rigid regions for the 3D cavity problem are shown in Fig. 5 ( $h = \frac{1}{64}$ ). The

regions are growing when the stress yield increases. The shape of the center region is somewhat different from the 2D case.

**References**

- [1] E. Barragy, G.F. Carey, Stream function-vorticity driven cavity solution using p finite elements, *Comput. Fluids* 26 (1997) 453–468.
- [2] I.E. Barton, R. Kirby, Finite difference scheme for the solution of fluid problems on non-staggered grids, *Int. J. Numer. Methods Fluids* 33 (2000) 939–959.
- [3] R. Becker, M. Braak, A finite element pressure gradient stabilization for the Stokes equations, *Calcolo* 28 (2001) 173–179.
- [4] M. Benzi, G.H. Golub, J. Liesen, Numerical solution of saddle point problems, *Acta Numer.* 14 (2005) 1–137.
- [5] M. Bercovier, M. Engelman, A finite element method for incompressible non-newtonian flows, *J. Comput. Phys.* 36 (1980) 313–326.
- [6] S. Berrone, Adaptive discretization of the Navier Stokes equations by stabilized finite element methods, *Comput. Methods Appl. Mech. Engrg.* 190 (2001) 4435–4455.
- [7] J.M. Boland, R.A. Nicolaides, On the stability of bilinear-constant velocity-pressure finite elements, *Numer. Math.* 44 (1984) 219–222.
- [8] O. Botella, R. Peyret, Benchmark spectral results on the lid-driven cavity flow, *Comput. Fluids* 27 (1998) 421–433.
- [9] P.B. Bochev, C.R. Dohrmann, M.D. Gunzburger, Stabilization of low-order mixed finite elements for the Stokes equations, *SIAM J. Numer. Anal.* 44 (2006) 82–101.
- [10] F. Brezzi, M. Fortin, *Mixed and Hybrid Finite Element Methods*, Springer, New York, 1991.
- [11] F. Brezzi, J. Pitkaranta, On the stabilization of Finite Element approximations of the Stokes problem, in: W. Hackbush (Ed.), *Efficient Solutions of Elliptic Systems*, Notes on Numerical Fluid Mechanics, vol. 10, Vieweg, Braunschweig, 1984, pp. 11–19.

- [12] A.G. Churbanov, A.N. Pavlov, P.N. Vabishchevich, Operator-splitting methods for the incompressible Navier–Stokes equations on non-staggered grids. Part 1: First-order schemes, *Int. J. Numer. Meth. Fluids* 21 (1995) 617–640.
- [13] E.J. Dean, R. Glowinski, G. Guidoboni, On the numerical simulation of Bingham visco-plastic flow: old and new results, *J. Non-Newton. Fluid Mech.* 142 (2007) 36–62.
- [14] G. Duvaut, J.L. Lions, *Inequalities in Mechanics and Physics*, Springer, 1976.
- [15] R.N. Elias, M.A.D. Martins, A.L.G.A. Coutinho, Parallel edge-based solution of viscoplastic flows with the SUPG/PSPG formulation, *Comput. Mech.* 38 (2006) 365–381.
- [16] H.C. Elman, D.J. Silvester, A.J. Wathen, *Finite Elements and Fast Iterative Solvers: With Applications in Incompressible Fluid Dynamics*, Numerical Mathematics and Scientific Computation, Oxford University Press, Oxford, UK, 2005.
- [17] M. Fortin, R. Peyret, R. Temam, Resolution numerique des equations de Navier–Stokes pour un fluide incompressible, *J. Mech.* 10 (1971) 357–390.
- [18] R. Glowinski, J.L. Lions, R. Tremolieres, *Numerical Analysis of Variational Inequalities*, Studies in Mathematics and its Applications, vol. 8, North-Holland, Amsterdam, 1981.
- [19] R. Glowinski, *Numerical Methods for Nonlinear Variational Problems*, Springer-Verlag, New York, 1984.
- [20] L.P. Franca, R. Stenberg, Error analysis of some Galerkin least-squares methods for the elasticity equations, *SIAM J. Numer. Anal.* 28 (1991) 1680–1697.
- [21] W. Hackbusch, *Iterative Solution of Large Sparse Systems of Equations*, Springer, New York, 1994.
- [22] E. Mitsoulis, Th. Zisis, Flow of Bingham plastics in a lid-driven cavity, *J. Non-Newton. Fluid Mech.* 101 (2001) 173–180.
- [23] E.A. Muravleva, M.A. Olshanskii, Two finite-difference schemes for the Bingham cavity flows, *Rus. J. Numer. Anal. Math. Model.* 23 (2008) 615–634.
- [24] W. Layton, Model reduction by constraints and an induced pressure stabilization, *J. Numer. Linear Alg. Appl.* 12 (2005) 547–562.
- [25] A. Ouazzi, S. Turek, J. Hron, Finite element methods for the simulation of incompressible powder flow, *Commun. Numer. Meth. Engrg.* 21 (2005) 581–596.
- [26] M.A. Olshanskii, Yu.V. Vassilevski, Pressure Schur complement preconditioners for the discrete Oseen problem, *SIAM J. Sci. Comput.* 29 (2007) 2686–2704.
- [27] J.R. Pacheco, A. Pacheco-Vega, T. Rodic, R.E. Peck, Numerical simulations of heat transfer and fluid flow problems using an immersed boundary method on non-staggered grids, *Numer. Heat Transfer, Part B* 48 (2005) 1–24.
- [28] T.C. Papanastasiou, Flows of materials with yield, *J. Rheol.* 31 (1987) 385–404.
- [29] S.V. Patankar, *Numerical Heat Transfer and Fluid Flow*, Hemisphere, Washington, DC, 1980.
- [30] J. Peters, V. Reichelt, A. Reusken, Fast iterative solvers for discrete Stokes equations, *SIAM J. Sci. Comput.* 27 (2005) 646–666.
- [31] F.J. Sanchez, Application of a first-order operator splitting method to Bingham fluid flow simulation, *Comput. Math. Appl.* 36 (1998) 71–86.
- [32] M. Sahin, H.J. Wilson, A semi-staggered dilation-free finite volume method for the numerical solution of viscoelastic fluid flows on all-hexahedral elements, *J. Non-Newton. Fluid Mech.* 147 (2007) 79–91.
- [33] W. Shyy, T.C. Vu, On the adoption of velocity variable and grid system for fluid flow computation in curvilinear coordinates, *J. Comput. Phys.* 92 (1991) 82–105.
- [34] R. Stenberg, Error analysis of some finite element methods for the Stokes problem, *Math. Comput.* 54 (1990) 495–508.
- [35] D. Vola, L. Boscardin, J.C. Latche, Laminar unsteady flows of Bingham fluids: a numerical strategy and some benchmark results, *J. Comput. Phys.* 187 (2003) 441–456.
- [36] M.C. Wendl, R.K. Agarawal, Mass conservation and the accuracy of non-staggered grid incompressible flow schemes, in: M.M. Hafez (Ed.), *Numerical Simulations of Incompressible Flows*, World Scientific, 2003.
- [37] T. Ye, R. Mittal, H.S. Udaykumar, W. Shyy, An accurate Cartesian grid method for viscous incompressible flows with complex immersed boundaries, *J. Comput. Phys.* 156 (1999) 209–240.